Nano Energy (2014) 7, 80–85

Available online at www.sciencedirect.com

ScienceDirect

journal homepage: www.elsevier.com/locate/nanoenergy

RAPID COMMUNICATION

# Cesium-doped methylammonium lead iodide perovskite light absorber for hybrid solar cells

Hyosung Choi, Jaeki Jeong, Hak-Beom Kim, Seongbeom Kim, Bright Walker, Gi-Hwan Kim, Jin Young Kim*

*School of Energy and Chemical Engineering, Ulsan National Institute of Science and Technology (UNIST), Ulsan 689-798, Republic of Korea*

Received 16 January 2014; received in revised form 30 March 2014; accepted 23 April 2014
Available online 6 May 2014

**KEYWORDS**
Methylammonium lead iodide perovskite;
Cesium doping;
Planar heterojunction;
Hybrid solar cells

**Abstract**
We demonstrate cesium-doping in methylammonium lead iodide perovskites ($Cs_xMA_{1-x}PbI_3$) light absorbers to improve the performance of inverted-type perovskite/fullerene planar heterojunction hybrid solar cells. $Cs_xMA_{1-x}PbI_3$ perovskite devices with an optimized 10% Cs doping concentration exhibit remarkable improvement in device efficiency from 5.51% to 7.68% due to increases in short-circuit current density and open-circuit voltage via increased light absorption at optimum device thickness, improved film morphology and a widening of the energy difference between the valence band of the perovskite and lowest unoccupied molecular orbital level of PCBM.


## Introduction

Organolead halide perovskites ($ABX_3$ where A is organic or inorganic cation, B is metal cation, and X is halogen anion) have been extensively investigated as light absorbers for high efficiency organic–inorganic hybrid solar cells (HSCs) over the last few years [1–8]. In particular, methylammonium lead halide perovskites ($MAPbX_3$) are regarded as particularly promising light absorbers due to their many advantages including optimal band gaps, high absorption coefficients, and long-range exciton diffusion lengths [1,4,5]. These perovskites have led to solar cells with power conversion efficiencies (PCEs) up to 15% in conjunction with the development of new device architectures (meso-structure metal oxides) [1,9,10], and deposition methods (such as sequential and vapor deposition) [2,3]. Although a few attempts to synthesize new perovskites have been made by changing halide anions (X) in the $MAPbX_3$ structure, these materials have not led to improvements in device efficiency [11–13]. Optical and electronic properties of organolead halide perovskites have been studied by replacing MA cation with other organic cations such as ethylammonium and formamidinium [14,15–17]. However, there has been no

*Corresponding author. Tel: +82 52 217 2911, fax: +82 52 217 2909.
*E-mail address:* jykim@unist.ac.kr (J.Y. Kim).

http://dx.doi.org/10.1016/j.nanoen.2014.04.017
2211-2855/

investigation of the effects that changing organic cation with inorganic cation in the $MAPbX_3$ structure has on properties of perovskite light absorbers. Thus, there is still considerable opportunity to improve device performance by optimizing optical and electronic properties of perovskite materials through study of the components and composition ratio.

Conventional perovskite-based HSCs (pero-HSCs) have employed meso-structured n-type metal oxide layer and organic hole conductors [1,9,18,19]. However, these devices require high temperature calcination (typically over 500 °C) of the compact titanium oxide layer or thermal evaporation under high vacuum for deposition of the perovskite layer [10,20]. High temperature thermal treatment and vacuum processing pose challenges for flexible device applications and roll-to-roll mass production. Although functioning inverted structures have been successfully realized using perovskite/fullerene planar heterojunctions [21-23], their performance can be further enhanced by improving the morphology of the perovskite films and developing new device architectures. Therefore, we seek to investigate simple and effective device processing procedures along with novel perovskite light absorbers for efficient pero-HSCs. Here, we report the synthesis of cesium (Cs)-doped methylammonium lead iodide ($Cs_xMA_{1-x}PbI_3$) perovskites as light absorbers and develop high-performance inverted-type planar heterojunction HSCs (iPH-HSCs) utilizing $Cs_xMA_{1-x}PbI_3$ as an electron donor and [6,6]-phenyl-$C_{60}$ butyric acid methyl ester (PCBM) as an electron acceptor.

The cation (A) in $ABX_3$ perovskites commonly comprises alkylammonium or alkali metal cations (e.g. methylammonium, formamidinium, cesium, etc.). The identity of the A cation strongly influences the band gap and electronic properties of perovskites through its influence on the crystal structure [24,25]. Since $MAPbI_3$ perovskite is a well-known light absorber with a low band gap of 1.5 eV and high extinction coefficient in pero-HSCs [1,9,26], we replace a fraction of the MA ions with Cs in order to optimize the optical and electrical properties of the material while maintaining the fundamental characteristics of $MAPbI_3$ (Figure 1a). For the preparation of $MAPbI_3$ absorbing films, a precursor solution consisting of equimolar amounts of methylammonium iodide (MAI) and lead iodide ($PbI_2$) was first dissolved in a mixed solvent of dimethylformamide (DMF) and γ-butyrolactone (GBL) (DMF:GBL=97:3 vol%), and stirred at 60 °C for 24 h in a nitrogen-filled glovebox. The $Cs_xMA_{1-x}PbI_3$ precursor solutions were prepared using same procedure with a fraction of the MAI being replaced by CsI.

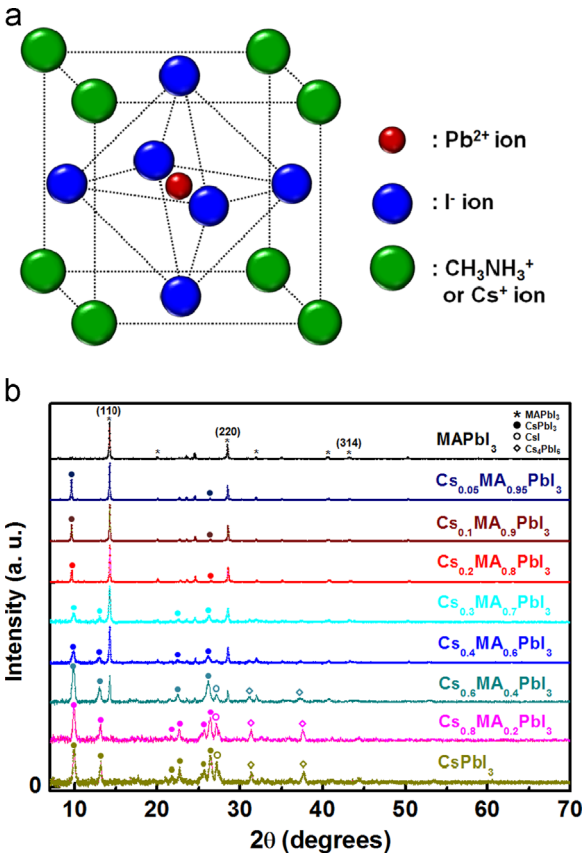


**Figure 1** (a) Crystal structure and (b) XRD patterns of $Cs_xMA_{1-x}PbI_3$ perovskites.

## Experimental section

### Preparation and characterization of perovskite

Cesium iodide (CsI), lead iodide ($PbI_2$), anhydrous *N*,*N*-dimethylformamide (DMF), and γ-butyrolactone (GBL) were purchased from Sigma-Aldrich and used without further purification. [6,6]-phenyl-$C_{60}$ butyric acid methyl ester (PCBM) was purchased from Rieke Metal Incorporation. Methyl ammonium iodide ($CH_3NH_3I$) was synthesized using a previously reported method [23]. Precursor solutions of $Cs_xMA_{1-x}PbI_3$ were prepared by dissolving equimolar amounts of $CsI:CH_3NH_3I$ and $PbI_2$ in a mixed solvent consisting of DMF:GBL (97:3 [vol%]) at a concentration of 120 mg/ml. Solutions were stirred at 60 °C for 12 h inside glovebox filled with nitrogen gas prior to use.

For scanning electron microscope measurements (SEM, NanoSEM 230, FEI), perovskite precursor solutions were coated onto Si substrates by spin-coating at various spin-rates and followed by drying at 110 °C for 10 min on a digital hotplate. For cross-sectional images of solar cells, 1.8 μm of carbon was deposited on top of the device to prevent sample damage and a focused ion beam was used to cut thin slices (300 nm thickness) of each sample with lengths and heights of 5 μm × 5 μm. High-resolution transmission electron microscopy (TEM, JEM-1400) was used to obtain cross-sectional images of the samples. For X-ray diffraction (XRD) measurements, perovskite films were coated on PEDOT:PSS-coated glass substrates and diffractograms were collected using a Bruker, D8 ADVANCE at a scan rate of 2.4° $min^{-1}$. UV-vis absorption was measured using a Varian Cary 5000 spectrophotometer. AFM images were obtained using a Veeco Multimode AFM microscope in a tapping mode.

### Device fabrication and characterization

ITO-coated glass substrates were cleaned by sequential ultrasonication in deionized water, acetone, and isopropanol for 10 min each. A solution of poly(3,4-ethylenedioxythiophene):polystyrene sulfonic acid (PEDOT:PSS) was spin-cast at 5000 rpm on UV ozone-treated ITO and dried at 140 °C for 10 min. On top of PEDOT:PSS layer, precursor

solutions of $Cs_xMA_{1-x}PbI_3$ perovskites (120 mg/ml) were spin-cast at 5000 rpm for 90 s and dried on hot-plate at 110 °C for 10 min. A PCBM solution (7 mg/ml) in chloroform was spin-cast at 3000 rpm on top of perovskite layer. Subsequently, an Al (100 nm) electrode was deposited layer under vacuum ($<10^{-6}$ Torr) on top of the PCBM by thermal evaporation. The current density-voltage (*J-V*) characteristics of PSCs were measured using a Keithley 2635A Source Measure Unit. Solar cell performance was carried out using an Air Mass 1.5 Global (AM 1.5 G) solar simulator with an irradiation intensity of 100 mW $cm^{-2}$. External quantum efficiency (EQE) measurements were obtained using a PV measurements QE system using monochromated light from a xenon lamp under ambient conditions. The monochromatic light intensity was calibrated with a Si photodiode and chopped at 100 Hz. Masks (13.0 $mm^2$) made of thin metal were attached to each cell before measurement for *J-V* characteristics and EQE.

## Results and discussion

As shown in Figure 1a, the similar size of Cs and MA cations allows the Cs ions to substitute and coexist with MA ions in the cubo-octahedral 'A' sites of the octahedral unit cell without fundamentally changing the crystal structure. In order to quantify the effect of Cs incorporation on crystal structure, we collected X-ray diffractograms (XRD) of $Cs_xMA_{1-x}PbI_3$ perovskite films with different Cs ratios deposited on poly(3,4-ethylenedioxythio-phene):polystyrene sulfonic acid (PEDOT:PSS)-coated glass substrates (Figure 1b). The pure $MAPbI_3$ film exhibited diffraction peaks at $2\theta$ values of 14.15°, 20.05°, 28.47°, 31.94°, 40.66°, and 43.12°, corresponding to the (110), (112), (220), (310), (224), and (314) crystal planes of tetragonal perovskite, respectively [27]. However, there was absence of several diffraction peaks including the peak corresponding to (310) crystal plane, which may be attributed to preferred growth orientation during the formation of perovskite films [13,14,27,28]. For pure $CsPbI_3$ film, we observed strong diffraction peaks at 9.82°, 13.07°, 22.72°, 25.70°, and 26.39°, indicating an orthorhombic crystal structure [29,30]. There were negligible differences in diffraction peaks of films between pure $CsPbI_3$ and $Cs_xMA_{1-x}PbI_3$ perovskite with 80% Cs, whereas XRD peaks corresponding to the $MAPbI_3$ phase are clearly seen for $0 \le x \le 0.6$. The intensities of XRD peaks gradually increased for the $CsPbI_3$ composition and decreased for the $MAPbI_3$ composition upon increasing the Cs ratio in $Cs_xMA_{1-x}PbI_3$. It is worth noting that the XRD patterns clearly showed both $MAPbI_3$ and $CsPbI_3$ crystal phases for $Cs_xMA_{1-x}PbI_3$ perovskite from $x$=0.05 to 0.6, which imply that both crystal phases exist in the film upon substitution of MA with Cs. Additionally, the width of the diffraction peaks is observed to increase as the Cs content increases, indicating a reduction in the size of crystal domains upon Cs incorporation.

To investigate the change in optical properties of perovskite as a function of Cs content, UV-vis absorption and XRD patterns were collected for films with the composition $Cs_xMA_{1-x}PbI_3$ in which $x$ was varied from 0 to 1 (Figure 2a). Pure $MAPbI_3$ ($x$=0) and $CsPbI_3$ ($x$=1) absorb light in the visible and UV wavelength regions, respectively, due to their different optical band gaps [16,26,29,31]. Increasing the amount of Cs increases absorption in the range of 300-400 nm and decreases absorption in the range of 450-800 nm. Perovskite films with more than 30% Cs substitution exhibit a unique absorption peak at 420 nm characteristic of $CsPbI_3$, indicating that optical properties begin to reflect the $CsPbI_3$ phase for $x>0.3$. Transformed Kubelka-Munk spectra from UV-vis absorption results clearly showed the changes in optical band gap of $Cs_xMA_{1-x}PbI_3$ perovskite with different Cs ratio (Figure 2b). Optical band gap of $Cs_xMA_{1-x}PbI_3$ perovskite gradually increased from 1.52 eV for pure $MAPbI_3$ to 2.05 eV for pure $CsPbI_3$ with increasing Cs content (Table S1), which imply that optical band gap can be easily tuned by controlling the amount of Cs in $Cs_xMA_{1-x}PbI_3$ films.

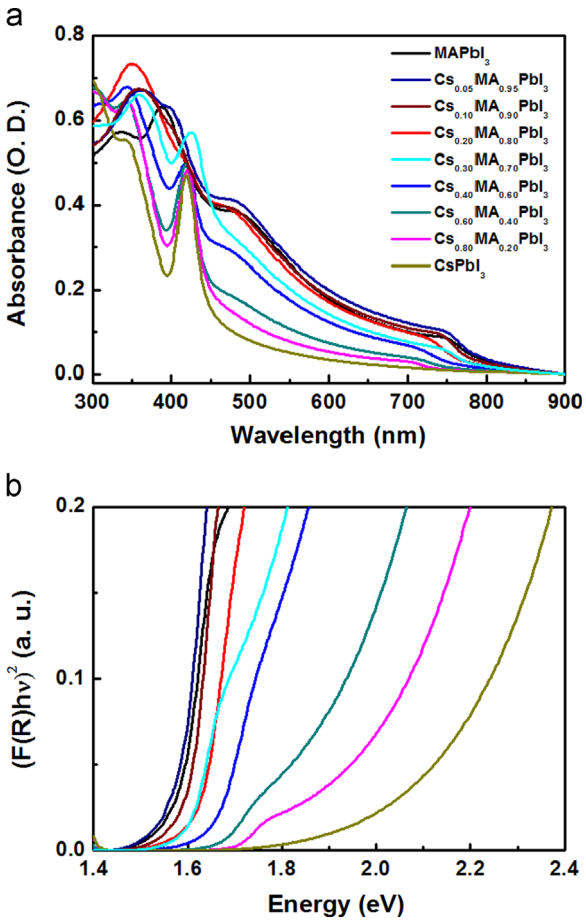


**Figure 2** (a) UV-vis absorption and (b) transformed Kubelka-Munk spectra of $Cs_xMA_{1-x}PbI_3$ perovskite films with different Cs ratio.

To clarify the differences between the morphologies of $MAPbI_3$ and $Cs_{0.1}MA_{0.9}PbI_3$ perovskite films, we collected scanning electron microscopy (SEM) and atomic force microscopy (AFM) images of the films. In the SEM top-view images (Figure S1a and S1b), both perovskite films exhibit typical patterns of perovskite crystals, comprising uniform crystal domains with grain sizes of less than 100 nm. In both cases, the perovskite layer completely covers the underlying PEDOT:PSS layer. These uniform morphologies are consistent with AFM topography images (Figure S1c and S1d). Both films exhibit smooth surfaces with root-mean-square

(rms) roughnesses of 6.60 nm for $MAPbI_3$ and 8.08 nm for $Cs_xMA_{1-x}PbI_3$. In order to confirm the incorporation of Cs in the $Cs_{0.1}MA_{0.9}PbI_3$ films, we also performed elemental mapping using energy dispersive spectroscopy (EDS). Figure S2a and S2b show the components of $MAPbI_3$ and $Cs_{0.1}MA_{0.9}PbI_3$ such as carbon (C), nitrogen (N), lead (Pb), iodine (I), and cesium (Cs). The EDS measurement for $Cs_{0.1}MA_{0.9}PbI_3$ perovskite films detected Cs element along with the same elements observed in $MAPbI_3$ perovskite (Figure S2b). The detailed weight and atomic percentages of chemical elements in $MAPbI_3$ and $Cs_{0.1}MA_{0.9}PbI_3$ perovskite are summarized in Table S2.

To evaluate the effect of Cs doping on device performance, we fabricated devices in the configuration of indium tin oxide (ITO)/PEDOT:PSS/perovskite/PCBM/Al. We employed perovskite films with different amounts of Cs in order to optimize Cs content for solar cell performance. Figure 3a and b shows the current density versus voltage (*J-V*) curves and external quantum efficiency (EQE) of iPH-HSCs utilizing $Cs_xMA_{1-x}PbI_3$ perovskite films as both light absorbers and electron donors. The device with pure $MAPbI_3$ perovskite exhibits a short-circuit current density ($J_{SC}$) of 8.89 mA $cm^{-2}$, an open-circuit voltage ($V_{OC}$) of 0.89 V, and a fill factor (*FF*) of 0.70, resulting in a power conversion efficiency (PCE) of 5.51%. In contrast, we obtained poor device performance in the device with pure $CsPbI_3$ ($J_{SC}$: 0.26 mA $cm^{-2}$, $V_{OC}$: 0.79 V, *FF*: 0.45, and PCE: 0.09%). Efficiencies of devices with $Cs_xMA_{1-x}PbI_3$ films started to decrease for $x > 0.1$, which can be attributed to relatively wider band gap of $CsPbI_3$ and the presence of extraneous crystal phases (CsI, $PbI_2$, and $Cs_4PbI_6$). It is worth noticing that the devices with $Cs_xMA_{1-x}PbI_3$ had high $V_{OC}$ values over 1.0 V for $0.05 \leq x \leq 0.6$. A small amount of Cs doping (below 10%) leads to remarkable improvement in device performance. The composition with 10% Cs leads to the best performance. The optimized device with $Cs_{0.1}MA_{0.9}PbI_3$ produced a $J_{SC}$ of 10.10 mA $cm^{-2}$, a $V_{OC}$ of 1.05 V, and *FF* of 0.73, yielding a PCE of 7.68%. The increase in device efficiency is largely due to ~14% and ~18% enhancements in $J_{SC}$ and $V_{OC}$, respectively, compared to those of the device with $MAPbI_3$. Detailed device characteristics are summarized in Table 1. The $V_{OC}$ value is determined by the energy difference between highest occupied molecular orbital (HOMO) or valence band (VB) of electron donor and lowest unoccupied molecular orbital (LUMO) or conduction band (CB) of electron acceptor ($E_{D(HOMO\ or\ VB)} - E_{A(LUMO\ or\ CB)}$) in heterojunction solar cells [22,32,33]. The $E_{D(VB)} - E_{A(LUMO)}$ of perovskite/PCBM HSCs is about 1.1 eV, indicating that $V_{OC}$ values can be improved by Cs doping. The increase in $V_{OC}$ to over 1 V may be attributed to a change in the quasi-Fermi energy of 0.10 eV at the perovskite/anode interface due to Cs doping of the perovskite phase, which increases the energy difference relative to the LUMO of PCBM, increasing the potential developed across the junction and leading to a higher $V_{OC}$ (Figure S3 and Table S3). The VB value of $MAPbI_3$ obtained from ultraviolet photoelectron spectroscopy (UPS) is in good agreement with previously report values [26]. In Figure 3b, we compare the EQE curves of $Cs_xMA_{1-x}PbI_3$ devices with different Cs ratios. The device with pure $MAPbI_3$ exhibits broad EQE in the range of 300-800 nm with a peak of 53.5% at 470 nm. The devices with $Cs_xMA_{1-x}PbI_3$ perovskite films for $x \leq 0.4$ exhibit a specific peak around

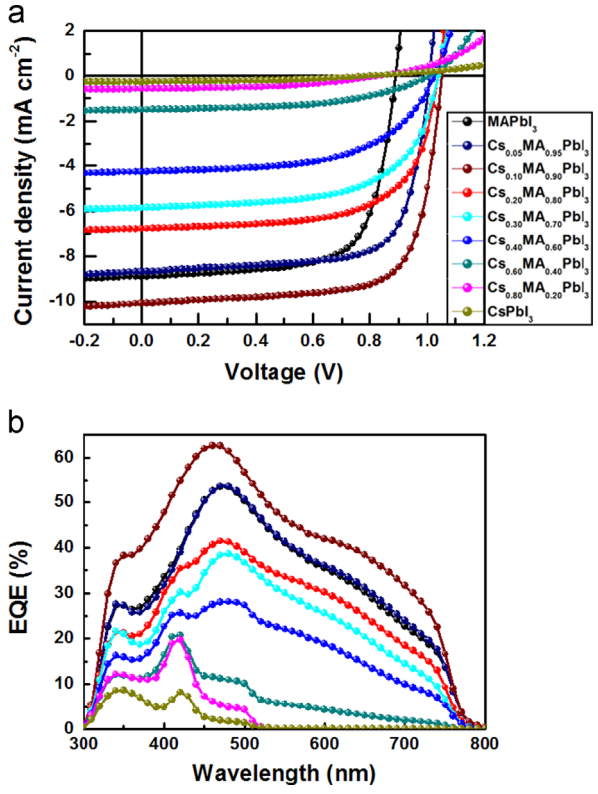


**Figure 3** (a) *J-V* characteristics and (b) EQE of $Cs_xMA_{1-x}PbI_3$ perovskite devices with different Cs ratio.

**Table 1** Characteristics of $Cs_xMA_{1-x}PbI_3$ perovskite devices with different Cs ratio.

| Perovskite | $J_{SC}$ (mA $cm^{-2}$) | $V_{OC}$ (V) | *FF* | PCE (%) | $J_{SC}$ [Cal.] (mA/$cm^2$) |
|---|---|---|---|---|---|
| $MAPbI_3$ | 8.89 | 0.89 | 0.70 | 5.51 | 8.55 |
| $Cs_{0.05}MA_{0.95}PbI_3$ | 8.69 | 1.01 | 0.72 | 6.29 | 8.68 |
| $Cs_{0.10}MA_{0.90}PbI_3$ | 10.10 | 1.05 | 0.73 | 7.68 | 10.22 |
| $Cs_{0.20}MA_{0.80}PbI_3$ | 6.76 | 1.04 | 0.65 | 4.58 | 6.92 |
| $Cs_{0.30}MA_{0.70}PbI_3$ | 5.85 | 1.04 | 0.62 | 3.78 | 5.97 |
| $Cs_{0.40}MA_{0.60}PbI_3$ | 4.26 | 1.03 | 0.57 | 2.50 | 4.44 |
| $Cs_{0.60}MA_{0.40}PbI_3$ | 1.50 | 1.01 | 0.52 | 0.79 | 1.51 |
| $Cs_{0.80}MA_{0.20}PbI_3$ | 0.58 | 0.84 | 0.46 | 0.22 | 0.65 |
| $CsPbI_3$ | 0.26 | 0.79 | 0.45 | 0.09 | 0.28 |

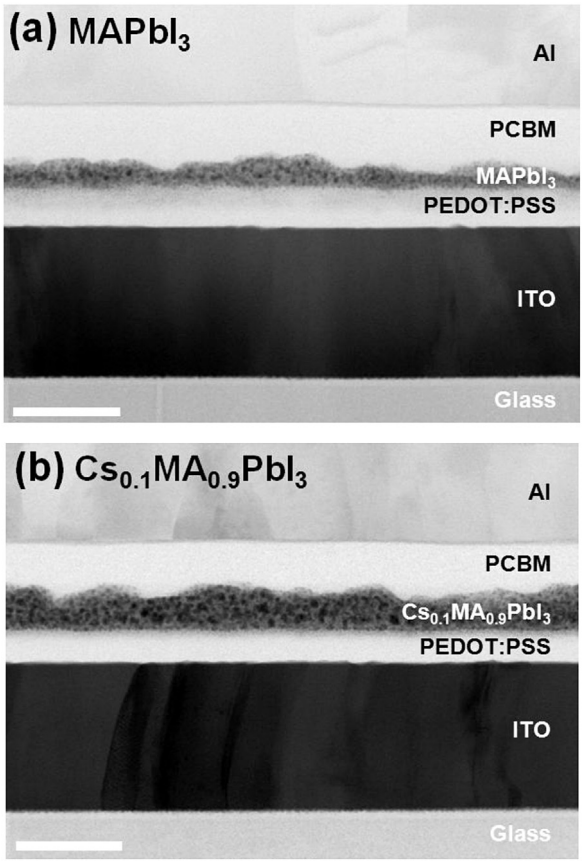


**Figure 4** Cross-sectional TEM images of the devices with (a) $MAPbI_3$ and (b) $Cs_{0.1}MA_{0.9}PbI_3$ perovskite films as light absorber. Scale bar is 100 nm.

470 nm, whereas a peak at 420 nm gradually increases for $x > 0.2$. In particular, the EQE values decrease significantly in the longer wavelength region above 430 nm upon increasing Cs ratio. These tendencies are consistent with the UV-vis absorption spectra of the films (Figure 2a). The best device, with a composition $Cs_{0.1}MA_{0.9}PbI_3$ shows the highest EQE values over the entire visible spectrum with a maximum of 62.6% at 470 nm. This $J_{SC}$ enhancement results from improved light absorption at optimal device thickness (Figure S4); differences in the absorption spectra of the two perovskite films are in good agreement with the observed increase in EQE with 10% Cs doping (Figure S5). Although we tested long-term stability of the devices with $MAPbI_3$ and $Cs_{0.1}MA_{0.9}PbI_3$ perovskite in ambient conditions (temperature: 20 °C, humidity: 11%), both devices exhibited poor stability due to the acidic nature of PEDOT:PSS and easily-oxidized Al electrode which were used (Figure S6).

Figure 4 shows cross-sectional transmission electron microscopy (TEM) images of optimized devices with $MAPbI_3$ and $Cs_{0.1}MA_{0.9}PbI_3$ perovskites. Each layer and corresponding thickness can clearly be seen in these images (average thickness of ITO: 140 nm, PEDOT:PSS: 35 nm, PCBM: 50 nm, and Al: 100 nm). We find that the optimal device thickness of $MAPbI_3$ perovskite ($30 \pm 11$ nm) (Figure 4a) is thinner than $Cs_{0.1}MA_{0.9}PbI_3$ ($38 \pm 9$ nm) (Figure 4b), indicating that the improved $J_{SC}$ in the $Cs_{0.1}MA_{0.9}PbI_3$ film is partially due to a thicker film. Compared to the device with $MAPbI_3$, the higher *FF* of the device using $Cs_{0.1}MA_{0.9}PbI_3$ can be attributed to a better contact at the perovskite/PCBM and PCBM/Al interfaces due to the more even surface of the $Cs_{0.1}MA_{0.9}PbI_3$ film and smoother surface after PCBM coating (Figure S7).

## Conclusions

In conclusion, we synthesized a series of perovskite light absorbers with the composition $Cs_xMA_{1-x}PbI_3$ and evaluated their performance in inverted-type perovskite/PCBM hybrid solar cells. High performance was achieved via 10% Cs doping in the $MAPbI_3$ perovskite structure, resulting in a ~40% enhancement in device efficiency via improvement in light absorption and morphology as well an increased energy difference between the valance band of the perovskite and LUMO level of PCBM. Our approach to perovskite design offers the possibility to enhance the performance of conventional perovskite solar cells with n-type titania or alumina layers and to achieve even higher open-circuit voltages by employing tandem device structures.

## Acknowledgments

H. Choi, J. Jeong, and H.-B. Kim contributed equally to this work. This research was supported by the National Research Foundation of Korea Grant (NRF-2009-0093020, NRF-2013R1A2A2A01015342) and the BK21 Plus funded by the Ministry of Education, Republic of Korea (10Z20130011057).

## Appendix A. Supporting information

Supplementary data associated with this article can be found in the online version at http://dx.doi.org/10.1016/j.nanoen.2014.04.017.

## References

[1] M.M. Lee, J. Teuscher, T. Miyasaka, T.N. Murakami, H. J. Snaith, Science 338 (2012) 643-647.
[2] J. Burschka, N. Pellet, S.-J. Moon, R. Humphry-Baker, P. Gao, M.K. Nazeeruddin, M. Gratzel, Nature 499 (2013) 316-319.
[3] M. Liu, M.B. Johnston, H.J. Snaith, Nature 501 (2013) 395-398.
[4] S.D. Stranks, G.E. Eperon, G. Grancini, C. Menelaou, M.J. P. Alcocer, T. Leijtens, L.M. Herz, A. Petrozza, H.J. Snaith, Science 342 (2013) 341-344.
[5] G. Xing, N. Mathews, S. Sun, S.S. Lim, Y.M. Lam, M. Grätzel, S. Mhaisalkar, T.C. Sum, Science 342 (2013) 344-347.
[6] I. Chung, B. Lee, J. He, R.P.H. Chang, M.G. Kanatzidis, Nature 485 (2012) 486-489.
[7] J.-H. Im, C.-R. Lee, J.-W. Lee, S.-W. Park, N.-G. Park, Nanoscale 3 (2011) 4088-4093.
[8] A. Kojima, K. Teshima, Y. Shirai, T. Miyasaka, J. Am. Chem. Soc. 131 (2009) 6050-6051.
[9] J.H. Heo, S.H. Im, J.H. Noh, T.N. Mandal, C.-S. Lim, J. A. Chang, Y.H. Lee, H.-j. Kim, A. Sarkar, K. NazeeruddinMd, M. Gratzel, S.I. Seok, Nat. Photon. 7 (2013) 486-491.
[10] J.M. Ball, M.M. Lee, A. Hey, H.J. Snaith, Energy Environ. Sci. 6 (2013) 1739-1743.
[11] M.D. Perez, C. Borek, S.R. Forrest, M.E. Thompson, J. Am. Chem. Soc. 131 (2009) 9281-9286.
[12] J.H. Noh, S.H. Im, J.H. Heo, T.N. Mandal, S.I. Seok, Nano Lett. 13 (2013) 1764-1769.

[13] E. Edri, S. Kirmayer, D. Cahen, G. Hodes, J. Phys. Chem. Lett. 4 (2013) 897–902.
[14] J.-H. Im, J. Chung, S.-J. Kim, N.-G. Park, Nanoscale Res. Lett. 7 (2012) 353.
[15] T.M. Koh, K. Fu, Y. Fang, S. Chen, T.C. Sum, N. Mathews, S. G. Mhaisalkar, P.P. Boix, T. Baikie, J. Phys. Chem. C (2013). http://dx.doi.org/10.1021/jp411112k.
[16] G.E. Eperon, S.D. Stranks, C. Menelaou, M.B. Johnston, L. M. Herz, H.J. Snaith, Energy Environ. Sci. 7 (2014) 982–988.
[17] S. Pang, H. Hu, J. Zhang, S. Lv, Y. Yu, F. Wei, T. Qin, H. Xu, Z. Liu, G. Cui, Chem. Mater. 26 (2014) 1485–1491.
[18] L. Etgar, P. Gao, Z. Xue, Q. Peng, A.K. Chandiran, B. Liu, M. K. Nazeeruddin, M. Grätzel, J. Am. Chem. Soc. 134 (2012) 17396–17399.
[19] D. Bi, L. Yang, G. Boschloo, A. Hagfeldt, E.M.J. Johansson, J. Phys. Chem. Lett. 4 (2013) 1532–1536.
[20] M.J. Carnie, C. Charbonneau, M.L. Davies, J. Troughton, T. M. Watson, K. Wojciechowski, H. Snaith, D.A. Worsley, Chem. Commun. 49 (2013) 7893–7895.
[21] P. Docampo, J.M. Ball, M. Darwich, G.E. Eperon, H.J. Snaith, Nat. Commun. 4 (2013) 2761.
[22] S. Sun, T. Salim, N. Mathews, M. Duchamp, C. Boothroyd, G. Xing, T.C. Sum, Y.M. Lam, Energy Environ. Sci. 7 (2014) 399–407.
[23] J.-Y. Jeng, Y.-F. Chiang, M.-H. Lee, S.-R. Peng, T.-F. Guo, P. Chen, T.-C. Wen, Adv. Mater. 25 (2013) 3727–3732.
[24] T. Baikie, Y. Fang, J.M. Kadro, M. Schreyer, F. Wei, S. G. Mhaisalkar, M. Graetzel, T.J. White, J. Mater. Chem. A 1 (2013) 5628–5641.
[25] D.B. Mitzi, J. Mater. Chem. 14 (2004) 2355–2365.
[26] H.-S. Kim, C.-R. Lee, J.-H. Im, K.-B. Lee, T. Moehl, A. Marchioro, S.-J. Moon, R. Humphry-Baker, J.-H. Yum, J. E. Moser, M. Gratzel, N.-G. Park, Sci. Rep. 2 (2012) 591.
[27] Y. Zhao, K. Zhu, J. Phys. Chem. Lett. 4 (2013) 2880–2884.
[28] G.E. Eperon, V.M. Burlakov, P. Docampo, A. Goriely, H. J. Snaith, Adv. Funct. Mater. 24 (2014) 151–157.
[29] C.C. Stoumpos, C.D. Malliakas, M.G. Kanatzidis, Inorg. Chem. 52 (2013) 9019–9038.
[30] M. Nikl, K. Nitsch, J. Chval, F. Somma, A.R. Phani, S. Santucci, C. Giampaolo, P. Fabeni, G.P. Pazzi, X.Q. Feng, J. Phys.: Condens. Matter 12 (2000) 1939.
[31] S. Kondo, A. Masaki, T. Saito, H. Asada, Solid State Commun. 124 (2002) 211–214.
[32] C.J. Brabec, A. Cravino, D. Meissner, N.S. Sariciftci, T. Fromherz, M.T. Rispens, L. Sanchez, J.C. Hummelen, Adv. Funct. Mater. 11 (2001) 374–380.
[33] N. Beaumont, I. Hancox, P. Sullivan, R.A. Hatton, T.S. Jones, Energy Environ. Sci. 4 (2011) 1708–1711.

**Dr. Hyosung Choi** received B.S. at Pusan National University in Organic Material Science & Engineering (2003–2007), M.S. at GIST in Materials Science & Engineering (2007–2009), Ph.D. at UNIST in Energy Engineering (2010–2013). His research interests include polymer solar cells and Hybrid solar cells. E-mail: bestprofitw@unist.ac.kr

**Jaeki Jeong** received B.S. at Pusan National University in Physics (2010), M.S. at Pusan National University in Physics (2012), Doctoral Program (2013-present). His research interest includes perovskite solar cells. E-mail: jekichaki@gmail.com

**Hak-beom Kim** received B.S. at Hongik University in Ceramic Engineering (2005-2011). He was a Researcher (2011–2012) and pursuing Combined Master's-Doctoral Program (2012-present). His research interest includes perovskite solar cells.
E-mail: asinlim@unist.ac.kr

**Dr. Seongbeom Kim** received B.S. (2004), M.S. (2006) and Ph.D. (2012) at KAIST. His research interest includes and organic-inorganic solar cells, organic electronics, fabrication of nanoparticles using laser and plasma, and laser processing.
E-mail: kimseongbeom@kaist.ac.kr

**Dr. Bright J. Walker** received B.S. at University of California, Berkeley (2003), Ph.D. at University of California, Santa Barbara (2012). He is a Post-Doctoral Researcher at Ulsan National Institute of Science and Technology (2011-present).

**Gi-Hwan Kim** received B.S. at Kum oh National Institute of Technology in Polymer Engineering (2009), Combined Master's-Doctoral Program (2009-present). His research interest includes colloidal quantum dot solar cells and thin film field-effect transistors. E-mail: genius1020@unist.ac.kr

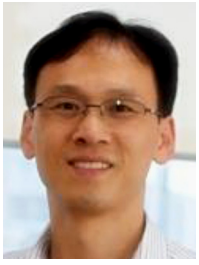

**Prof. Jin Young Kim** is an Associate Professor Department of Energy Engineering. He received his Ph.D. in Physics from Pusan National University (2000.09-2005.02), M.S. in Physics from Pusan National University (1998.09-2000.08) and B.S. in Physics from Pusan National University (1992.03-1998.08). He is an Associate Professor, in the Department of Energy Engineering, Ulsan National University of Science and Technology, Ulsan, Korea (2008.07-present). He served as an Assistant Research Professor, in the Heeger Center for Advanced Materials, Gwangju Institute of Science and Technology (GIST), Gwangju, Korea (2007.07-2008) and he was a Post Doc. Researcher, in the Center for Polymers and Organic Solids, UC Santa Barbara, Santa Barbara, US (Prof. A. J. Heeger) (2005.04-2007.07).